

The Southern Galactic Plane Survey: H I Observations and Analysis

N. M. McClure-Griffiths,¹ John M. Dickey,^{2,3} B. M. Gaensler,⁴ A. J. Green,⁵ Marijke Haverkorn,⁴ and S. Strasser²

ABSTRACT

We describe the H I component of the Southern Galactic Plane Survey (SGPS). The SGPS is a large-scale project to image at arcminute resolution the H I spectral line and 21 cm continuum emission in parts of the plane of the Milky Way. The survey covers Galactic longitudes $253^\circ \leq l \leq 358^\circ$ and latitudes $|b| \leq 1.5^\circ$ (SGPS I), plus a first quadrant extension covering $5^\circ \leq l \leq 20^\circ$ and $|b| \leq 1.5^\circ$ (SGPS II). The survey combines data from the Australia Telescope Compact Array and the Parkes Radio Telescope for sensitivity to angular scales ranging from 2 arcminutes to several degrees. The combined data cover 325 deg^2 and have an rms sensitivity of 1.6 K. Here we describe the H I observations and data reduction in detail, and present examples from the final data products. The complete dataset is publicly available through the Australia Telescope National Facility's H I Surveys archive. This dataset provides an unprecedented view of the neutral component of interstellar hydrogen in the inner Milky Way.

Subject headings: surveys — Galaxy: structure — ISM: structure — radio lines: ISM

¹Australia Telescope National Facility, CSIRO, PO Box 76, Epping NSW 1710, Australia; naomi.mcclure-griffiths@csiro.au

²Department of Astronomy, University of Minnesota, 116 Church St SE, Minneapolis, MN 55455; john@astro.umn.edu, strasser@astro.umn.edu

³Current address: School of Mathematics and Physics, University of Tasmania, Private Bag 21, Hobart TAS 7001, Australia

⁴Harvard-Smithsonian Center for Astrophysics, 60 Garden Street M S-6, Cambridge, MA 02138; bgaensler@cfa.harvard.edu, mhaverkorn@cfa.harvard.edu

⁵School of Physics, University of Sydney, NSW 2006, Australia; agreen@physics.usyd.edu.au

1. Introduction

The physics of the interstellar medium (ISM) is diverse and complicated. The cycle of stellar formation and death takes the ISM through a wide range of physical conditions, a number of which can be traced by the 21-cm hyperfine emission line produced by neutral hydrogen (H I). Tracing both structure and dynamics, H I is observed in emission and absorption, each probing different thermal states of the gas. Recent observations by Heiles & Troland (2003) and Dickey et al. (2003) show that H I observed in absorption traces gas with temperatures as cold as 15 K, whereas H I emission observations generally trace gas with temperatures in the range of few thousands (Dwarakanath et al. 2002). H I densities vary over a similarly broad range, from $\sim 10^{-2} \text{ cm}^{-3}$ in the diffuse warm neutral medium to $\sim 10^2 \text{ cm}^{-3}$ in regions of the cold neutral medium. The Milky Way provides an ideal laboratory in which to study the neutral ISM at sensitivities and spatial scales that are unattainable in external galaxies. Despite many years of observations of the ISM, our understanding of the medium is still simplistic, relying heavily on a three-phase model (e.g. McKee & Ostriker 1977). We have yet to adequately model the variety of temperatures, densities and structures known to exist in the ISM. Our lack of understanding is not only from the theoretical standpoint, but also from the lack of observational data probing H I physics over a wide range of spatial scales. It is clear that there is a great deal to learn about the structure, dynamics and thermal state of the neutral ISM from high resolution surveys of Galactic H I.

To reach this goal and develop a better understanding of the Galactic ISM the International Galactic Plane Survey (IGPS) is systematically imaging H I in the disk of the Milky Way. The IGPS consists of three individual surveys, the Canadian Galactic Plane Survey (CGPS; Taylor et al. 2003), the VLA Galactic Plane Survey (VGPS; Taylor et al. 2002), and the Southern Galactic Plane Survey (SGPS, described here). These surveys excel because of their exceptional spatial dynamic range, combining single dish and interferometer data for arcminute resolution imaging over areas of many degrees.

The Southern Galactic Plane Survey (McClure-Griffiths et al. 2001b) is a survey of the 21-cm continuum and H I spectral line emission in the fourth and parts of the first and third quadrants of the disk of the Milky Way. The survey provides a complete H I and 21 cm full polarization (Stokes I, Q, U, & V) dataset of the area $253^\circ \leq l \leq 358^\circ$, $b = \pm 1.5^\circ$ (SGPS I) and an extension into the first quadrant covering $5^\circ \leq l \leq 20^\circ$, $b = \pm 1.5^\circ$ (SGPS II). The SGPS is comprised of two surveys: a low resolution (FWHM = $15'$) survey completed with the Parkes 64m radio telescope and a high resolution (FWHM = $2'$) interferometric survey completed with the Australia Telescope Compact Array (ATCA). The data are combined to provide a dataset that is sensitive to more than two orders of magnitude in spatial scales. The combined data have an angular resolution of ~ 2 arcmin, spectral resolution of 0.8 km s^{-1}

and a sensitivity limit of ~ 1.6 K in the line. The main SGPS parameters are given in Table 7.

The scientific objectives of the SGPS are to provide a high-resolution 21cm polarized continuum and H I atlas of the Galactic plane with which to study the distribution and dynamics of both the warm and cool components of the ISM over size scales ranging from parsecs to kiloparsecs (McClure-Griffiths et al. 2001b; McClure-Griffiths 2001). Scientific results from the survey and its “test region” have been presented in a number of papers. An overview of the H I emission and absorption in the test region was published in McClure-Griffiths et al. (2001b). Other SGPS papers focusing on the test region data include an analysis of the H I emission spatial power spectrum (Dickey et al. 2001); a discussion of the abundance and temperature of cool H I clouds in the inner Galaxy (Dickey et al. 2003); an examination of extended polarized emission structure and rotation measures of point sources (Gaensler et al. 2001); and an analysis of rotation measure fluctuations indicating an outer scale for turbulence of ~ 2 pc (Haverkorn et al. 2004). Using the SGPS as a whole we have discovered a new, outer spiral arm in the fourth quadrant of the Milky Way (McClure-Griffiths et al. 2004); probed the physics of individual H I supershells (McClure-Griffiths et al. 2000, 2001a, 2003); discussed the Galactic distribution of H I supershells from a catalog of new supershells discovered in the SGPS (McClure-Griffiths et al. 2002); and explored the properties of H I self-absorption clouds discovered in the SGPS (Kavars et al. 2003, 2004).

Here we describe the SGPS in detail, focusing on the observing strategy and data reduction techniques. In particular, we describe the H I data; the continuum and polarization data require vastly different reduction techniques and will be described in a separate paper (M. Haverkorn et al. 2004, in preparation). This paper is organized as follows: in §2 we describe the low-resolution Parkes multibeam survey, in particular the data reduction strategies developed explicitly for this project. In §3 we describe the ATCA observations and data reduction, especially where the reduction deviates from standard techniques. The combination of our single dish and interferometer data is described in §4. Finally, the complete data products are described in §5 and representative images from the combined data cubes are presented in §5.2. The SGPS data are publicly available from the Australia Telescope National Facility (ATNF) H I Surveys archive.¹

¹<http://www.atnf.csiro.au/research/HI/common/>

2. Parkes Survey

The low resolution portion of the SGPS was observed with the Parkes Radio Telescope. This survey covers the area $253^\circ \leq l \leq 20^\circ$, $b = \pm 10^\circ$ with an angular resolution of $15'$. The Parkes survey was primarily designed to provide information about large scale structure not sampled in the ATCA survey. Expanding the latitude coverage of the Parkes survey to trace large-scale structures away from the Galactic plane provides additional information about the gas in a thicker disk and has led to the discovery of many new large H I shell structures (McClure-Griffiths et al. 2002). Therefore, the Parkes survey is released as a separate data product. Here we describe the observational and data reduction techniques used for this survey.

2.1. Observations

Single dish observations were made with the 21cm multibeam system at prime focus on the Parkes 64m Radio Telescope near Parkes, NSW, Australia. This is a focal plane array with thirteen independent feeds, each with dual, cryogenically cooled, orthogonal linear polarization receivers with stable, low system temperatures ($T_{sys} \sim 25$ K). The feeds are packed in a hexagonal pattern with a separation of $29'.1$ between the centers of adjacent feeds (Staveley-Smith et al. 1996). At $\lambda = 21$ cm the FWHM of the Parkes beam is $14'.4$, so the multibeam array does not fully sample the focal plane. For this project only the inner seven beams were used.

Data were obtained by mapping “on-the-fly”, driving the telescope at a constant Galactic longitude through 3 degrees of Galactic latitude at a rate of 1.1 deg min^{-1} . Data samples were written to disk every 5s. In order to maximize sky coverage and reduce redundant samples the multibeam receiver platform was rotated to maintain an angle of $19'.1$ between the face of the hexagon and the scan direction. The platform rotation results in seven parallel beam tracks, each separated by $9'.5$. To ensure Nyquist sampling, interleaved scans were made by offsetting the receiver package by 2.5 beam spacings and scanning in the opposite direction. The offset scans reduced the spacing between adjacent tracks to $4'.7$ and ensured that independent feeds are responsible for adjacent tracks. Along the scan direction the data samples are spaced by $\sim 5'.5$, which smears the beam slightly in the scan direction. In order to reduce the effects of variations in the system temperature with elevation, we made an effort to scan the telescope at a nearly constant zenith angle of approximately 30° .

Observations were conducted during five sessions between December 1998 and November 2000. The first set of observations on 15 and 16 December 1998 covered the ATCA survey

region of $253^\circ \leq l \leq 358^\circ$, $|b| \leq 1.5$. We conducted repeat observations of this same region at three month intervals for a year in order to reduce the annual variations in H I spectra due to stray radiation (Kalberla et al. 1980) and to improve the sensitivity of the observations. Ultimately the ATCA survey region was observed 10 times. During subsequent observing runs in June 1999, September 1999, and March 2000 the latitude range was extended to cover $|b| \leq 10^\circ$. Finally, between 28 October and 5 November 2000 the survey was extended through the Galactic Center to $l = 20^\circ$.

The data were recorded in frequency switched mode, switching in band between a center frequency of 1419.0 and 1422.125 MHz with every 5s cycle. We used the narrow-band multibeam correlator (Haynes et al. 1999), with a maximum bandwidth for each frequency of 8 MHz, with 2048 channels, giving a channel width of 3.9 kHz ($\Delta v = 0.82 \text{ km s}^{-1}$). After bandpass correction using frequency switched samples the usable bandwidth was approximately 4.5 MHz.

2.2. Bandpass and Brightness Temperature Calibration

The IAU standard narrow line calibration regions S6 and S9 were observed daily for absolute brightness temperature and bandpass calibration. For these observations each beam of the array was pointed on source for a 60s integration. These regions were also observed near a zenith angle of 30° so as not to compromise calibration with a significantly different gain and system temperature from the survey fields.

The bandpass shape is relatively stable over periods of days. However, there are variations in the front-end gain versus frequency shape on the timescale of seconds to minutes that can largely be removed by frequency switching. To remove the bandpass ripples, each spectrum was divided by the previous frequency switched sample to create a quotient spectrum. After this first reduction step, the shape of the quotient spectrum is stable to the 1-3% level over the course of a day. Next, the residual bandpass shape was corrected by dividing the quotient spectrum by a bandpass template. The bandpass template was determined daily for each beam and polarization from a time-averaged quotient spectrum on one of the standard line regions, S6 or S9. These spectra were normalized to a mean of one and then hand-fit by a series of Fourier components to create a bandpass template, $f(\nu)$. In general, the narrower line width of S6 ($\Delta v = 10.6 \text{ km s}^{-1}$ for S6, versus $\Delta v = 15.8 \text{ km s}^{-1}$ for S9) resulted in a better fit for the template.

In standard processing of H I single dish spectra the antenna temperature is calculated as $T_a = T'_{\text{sys}}(T_{\text{obs}} - T_{\text{ref}})T_{\text{ref}}^{-1}$, where T'_{sys} is the system temperature determined online during

the integration, T_{obs} is the observed spectrum and T_{ref} is the subsequent frequency-switched spectrum. The application of this technique, with some polynomial bandpass fitting, is relatively successful at removing ripples from the bandpass shape, but it also removes any continuum emission. For the SGPS we are interested in the continuum emission as well as the H I line so we employed a non-standard technique. For each spectrum we calculated the mean value, T_{bas} , of the reference spectrum over the area of the line, which should be the sum of the sky continuum temperature and the actual system temperature, T_{sys} . For T_{sys} we used an average system temperature calculated on the standard line regions, which we apply to an entire day’s observations. This is a generally valid assumption because the system temperature of the multibeam is extremely stable. The bandpass corrected spectra were then calculated as:

$$T_a(\nu) = T_{bas} \frac{T_{obs}(\nu)}{f(\nu) T'_{ref}(\nu)} - T_{sys} , \quad (1)$$

where $T'_{ref}(\nu)$ is a smoothed version of the frequency switched, or reference, spectrum. This technique differs from the standard single dish H I bandpass calibration because it only subtracts the absolute system temperature, not the sum of the system temperature and the continuum emission. The resultant spectra contain the observed continuum emission and have baselines that are typically flat to less than 1K. They are limited, however, by the accuracy in our determination of T_{sys} . The value of T_{sys} contains not only the receiving system temperature, but also the ground radiation temperature, which is elevation dependent and poorly known at 21 cm the for Parkes telescope. Because of the difficulty in estimating total power continuum levels with a single dish, T_{sys} is only accurate to $\sim 10 - 15\%$. Fortunately, for data products from which the continuum emission is subtracted later in the analysis this problem is alleviated.

After bandpass correction, the integral over part of the line on the standard regions was used to determine a calibration scale factor, C , to convert antenna temperature to absolute brightness temperature, $T_b = C T_a$. The calibration factor was calculated for each beam and each polarization by comparing the measured line integral on the standard line regions to the published Williams (1973) values for the line integral, such that $C = I_{true}/I_{obs}$. For S6 the line integral was calculated over the velocity range $-5.8 \text{ km s}^{-1} \leq v \leq +4.8 \text{ km s}^{-1}$ and is $I_{true} = 299 \text{ K km s}^{-1}$. The S9 line integral over the velocity range $+1.05 \text{ km s}^{-1} \leq v \leq +14.75 \text{ km s}^{-1}$ is $I_{true} = 953 \text{ K km s}^{-1}$. Using the line integral to scale the measured antenna temperature we find that the peak brightness temperature for S6 is $T_{max} = 57 \pm 2 \text{ K}$ and $T_{max} = 90 \pm 3 \text{ K}$ for S9. For comparison, another recent Parkes multibeam survey with a similar observational setup found $T_{max} = 83 \text{ K}$ for S9 (Brüns et al. 2003). The discrepancy may be due to the difference between the velocity range used for the line integral in Williams (1973), from which our calibration was derived and Kalberla et al. (1982), from which the Brüns et al. (2003) calibration was derived.

Finally, the spectra are shifted to the Local Standard of Rest (LSR) reference frame. The correction is calculated using standard techniques and is applied as a phase shift in the Fourier domain.

2.3. Imaging

The fully calibrated and velocity shifted Parkes spectra were imaged using *Gridzilla*, a gridding tool created for use with Parkes multibeam data and found in the ATNF subset of the *aips++* (now *casa*) package. The gridding algorithm is described in detail by Barnes et al. (2001). The SGPS data were gridded using a weighted median technique with a cellsize of $4'$, a Gaussian smoothing kernel of $16'$, and a smoothing kernel cutoff radius of $10'$. The Gaussian smoothing kernel and cutoff radius reduce the effective angular resolution of the gridded data to $\sim 16'$, which is slightly larger than the 14.4 FWHM of the Parkes beam at 1420 MHz. The effective resolution is estimated from Gaussian fits to point sources in the Parkes continuum images and to a beam map made on the calibration source PKS B1934-638. The imaged data were imported into the MIRIAD data reduction package (Sault & Killeen 2004) for further analysis and continuum subtraction. Image domain continuum subtraction was performed using a first order polynomial fit to the off-line channels.

3. Australia Telescope Compact Array Survey

The high resolution portion of the SGPS was completed with the Australia Telescope Compact Array (ATCA) synthesis imaging telescope. The ATCA survey is divided into two parts: SGPS I, covering the area $253^\circ \leq l \leq 358^\circ$, $|b| \leq 1.5$ and SGPS II, covering the area $5^\circ \leq l \leq 20^\circ$, $|b| \leq 1.5$. The Galactic center area from $358^\circ \leq l \leq 5^\circ$ has also been observed, but will be presented separately because it has a different observing and reduction strategy. Here we describe the observational and data reduction strategies used for both SGPS I and II.

3.1. Observations

The observations for SGPS I were conducted between December 1998 and August 2000, with re-observation of several areas in June 2001. SGPS II was observed between June and October 2002. The observational strategies are slightly different for the two data sets.

The ATCA is a six element interferometer near Narrabri, New South Wales, Australia.

It consists of five 22 m antennas that can be positioned along on a 3 km east-west track or a perpendicular 200 m north-south track and a sixth antenna fixed a further 3 km west of the end of the east-west track, for a maximum baseline of 6 km. The antennas can be arranged in a number of configurations. The SGPS takes advantage of the ATCA’s most compact configurations with maximum baselines (excluding the 6 km antenna) between 210 m and 750 m to maximize sensitivity to large scale structures. The array configurations used for SGPS I were: 210, 375, 750A, 750B, 750C, and 750D. The array configurations were chosen to ensure optimum sampling of the inner u - v plane and minimize redundant baselines. All baselines, in intervals of 15.5 m, from 31 m to 291 m, except 199m, are sampled. The long baselines of the 750-m arrays are poorly sampled and limit our practical resolution to $\sim 2'$. Before phase II of the SGPS the ATCA was upgraded to include a short north-south track and to add new stations on the east-west track that improve the coverage of the compact configurations. Because the SGPS II extends as far north as $\delta = -11^\circ$, the new north-south baselines were utilized to improve the u - v coverage and to reduce the effects of shadowing at low-elevations. The SGPS II was observed with the new EW352 and EW367 configurations, which give nearly complete coverage to baselines of 352 m in intervals of 15.5 m, and the north-south/east-west hybrid arrays, H75 and H168. Even with the hybrid arrays, the synthesized beam for the more northerly of the SGPS II fields is quite elliptical ($200'' \times 130''$).

In order to cover an area much larger than the primary beam of the ATCA antennas ($\Omega_{pb} = \lambda/D = 33'$), the survey was conducted as a mosaic of many pointings. The pointings were arranged in a hexagonal pattern with Nyquist spacing of 19 arcmin between adjacent pointings. The theoretical rms sensitivity for Nyquist sampled pointings is uniform to within $\leq 1\%$ across the entire observed area. In the SGPS I there are a total of 2212 pointings comprising twenty fields of 105 pointings and one field of 112 pointings. In the SGPS II there are 315 pointings divided in three fields of 105 pointings each. The fields composed of 105 pointings cover $5.5 \times 3^\circ$, centered on a Galactic latitude of $b = 0^\circ$. Each pointing was observed approximately 40 times with 30 second integrations for a total integration time of at least 20 minutes. The individual 30 second integrations are distributed evenly with hour angle. The exact u - v coverage varies from pointing to pointing, but is mostly constant within any given field. An example of the u - v coverage for one pointing near the center of the field at $l = 295^\circ$ is shown in Figure 1. The u - v coverage for this pointing is typical of the SGPS I fields. Similarly, an example of the u - v coverage for a pointing near the center of the field at $l = 12^\circ$ is shown in Figure 2. This coverage is typical of the SGPS II fields, although the coverage is much more circular for pointings near $l = 7^\circ$ and more elliptical for pointings near $l = 17^\circ$. The u - v coverage shown in Figure 2 differs from the coverage shown in Figure 1 because of the use of the north-south hybrid arrays in SGPS II.

The ATCA has linear feeds, receiving two orthogonal linear polarizations, X and Y , and is capable of observing two frequencies simultaneously. All data were recorded in a spectral line mode with 1024 channels across a 4 MHz bandwidth centered at 1420 MHz, and simultaneously a continuum mode with 32 channels across a 128 MHz bandwidth centered at 1384 MHz. In continuum mode the full polarization products, XX , YY , XY , and YX are recorded, whereas only the autocorrelations XX and YY are recorded in spectral line mode. Only the narrowband data are described here.

3.2. Calibration and Imaging

Data editing, calibration and imaging were conducted in the MIRIAD data reduction package using standard techniques (Sault & Killeen 2004). The primary flux calibrator for the southern hemisphere, PKS B1934-638, was observed at least once per day and was used for bandpass and absolute flux calibration of all data, assuming a flux at 1420 MHz of 14.86 Jy (Reynolds 1994). Observations of the secondary calibration sources PKS B0823-500, PKS B1105-680, PKS B1236-684, and PKS B1833-210 were used to solve for the time varying gain and delay corrections. One secondary calibrator was observed approximately every hour during the course of observations. The source PKS B0823-500 was observed for all fields between $l = 255^\circ$ and $l = 290^\circ$. PKS 1105-680 was observed for all fields from $l = 290^\circ$ to $l = 300^\circ$, and PKS 1236-684 was observed for all fields between $l = 300^\circ$ and $l = 320^\circ$. For fields between $l = 320^\circ$ and $l = 355^\circ$ PKS 1934-638 was used as both a primary and a secondary calibrator. Finally, PKS B1833-210 was used as the secondary calibrator for the three fields in SGPS II. In all cases, the gain solutions from the nearest secondary were copied to the SGPS field data. For fields flanked by two secondary calibrators the two solutions were merged when copied to the SGPS field.

The individual pointings of a field were linearly combined and imaged using a standard grid-and-FFT scheme. The mosaicing process uses the joint approach where dirty images of each pointing are linearly combined and then jointly deconvolved (Sault et al. 1996). This approach can offer a better deconvolution because information away from the pointing center is included in the deconvolution process. Additionally, this method takes best advantage of the mosaicing technique’s ability to recover information on angular scales larger than the scale determined by the minimum baseline separation, $\lambda/d_{\min} \sim 23'$, where d_{\min} is the minimum baseline. Jointly imaging and deconvolving the pointings increases the maximum angular scale imaged to $\lambda/(d_{\min} - D/2) \sim 36'$, where D is the diameter of a single antenna.

Super-uniform weighting was used for all H I cubes. Like uniform weighting, super-uniform weighting minimizes sidelobe levels to improve the dynamic range and sensitivity to

extended structures. However, uniform weighting reverts to natural weighting if the field of view is much larger than the primary beam, as is the case for large mosaics. Super-uniform weighting decouples the weighting from the field size and is therefore more successful than uniform weighting on large mosaics (Sault & Killeen 2004).

Two cubes of each imaged region were made: one containing continuum emission and one for which the continuum had been subtracted. For the continuum subtracted H I cubes, the continuum emission was subtracted from the calibrated u - v data prior to imaging (Sault 1994). These data were imaged without the 6 km antenna because of the poor sensitivity of the long baselines. For the continuum subtracted cubes, the pointings from two adjacent fields were jointly imaged to produce cubes covering $11^\circ \times 3^\circ$ ($l \times b$). For the H I cubes containing continuum emission the 6 km baselines were retained for use with H I absorption experiments. All cubes were then deconvolved using a maximum entropy deconvolution algorithm (Sault et al. 1996). The continuum-subtracted cubes for SGPS I were restored with a circular synthesized beam of $130''$. Because of their more northerly declinations, the SGPS II cubes are restored with slightly elliptical beams, $160'' \times 110''$ for field g010 and $200'' \times 130''$ for field g015. The SGPS I and II cubes with continuum emission and the 6 km antenna were restored with varying beam sizes, given in Table 4.

4. Single Dish and Interferometer Data Combination

Although mosaicing recovers information on larger angular scales than normal interferometric observations by reducing the effective shortest baseline, the ATCA images alone are not sensitive to angular scales larger than ~ 36 arcmin. In order to recover information on scales as large as the image size, we have combined the ATCA data with the Parkes data of the same region, which continuously sample the u - v plane between zero baseline separation and the 64 m diameter of the dish. There are a number of methods for combining single dish and interferometric data. The merits of the various methods have been discussed extensively by others, (e.g. Stanimirović 2002), so we will not repeat the discussion. For the SGPS we combine the data in the Fourier domain after deconvolution, as implemented in the MIRIAD task IMMERGE. We chose this combination method for several reasons, specifically that it is less sensitive than other methods to errors in the model for the Parkes beam, is not overly computationally intensive and produces reliable results. The ATCA and Parkes data are deconvolved separately, Fourier transformed, reweighted, linearly combined and then inverse Fourier transformed. If $V_{int}(k)$ is the Fourier transform of the deconvolved ATCA mosaic and $V_{sd}(k)$ is the Fourier transform of the deconvolved Parkes image, then the Fourier transform

of the combined image is given by

$$V_{comb}(k) = \omega'(k)V_{int}(k) + f_{cal}\omega''(k)V_{sd}(k). \quad (2)$$

The weighting functions, $\omega'(k)$ and $\omega''(k)$, are defined such that $\omega'(k) + \omega''(k)$ is a Gaussian whose full-width half-max is the same as the synthesized ATCA beam. In this way the ATCA data are downweighted on short baselines and the Parkes data are downweighted on the longer baselines. The calibration factor, f_{cal} , scales the Parkes data to match the brightness temperature scale of the ATCA data. This factor is determined by comparing the ATCA and Parkes datasets at every pixel and frequency in the range of overlapping spatial frequencies, which for an ATCA mosaic and a Parkes image is $\sim 120\lambda$ to $\sim 190\lambda$, where $\lambda = 21$ cm. For the SGPS we found that f_{cal} was equivalent to one to within 2%, which adds confidence to the calibration of the individual Parkes and ATCA datasets. The final combined H I cubes are regridded to Galactic coordinates with a Cartesian projection.

5. Resultant Data Products

There are three resultant H I data products: the Parkes H I cubes, ATCA+Parkes continuum subtracted H I cubes and ATCA+Parkes H I cubes with continuum emission. All three data products are available for viewing and downloading at the ATNF H I Surveys Archive at <http://www.atnf.csiro.au/research/HI/common>.

5.1. Parkes Data Cubes

Because the Parkes survey covers a much larger area than the ATCA survey these data are made available separately. The Parkes data are presented as twelve cubes, most covering $17^\circ \times 20^\circ$ ($l \times b$). Adjacent cubes overlap by about 4 degrees in longitude to allow for convenient subsequent combination. The center position, size and sensitivity of the Parkes cubes are given in Table 2. The final cubes have an angular resolution of $15'$ and a velocity resolution of 0.82 km s $^{-1}$. The rms noise in line-free channels is approximately 180 mK for the regions $1.5 \leq |b| \leq 10^\circ$, and approximately 60 mK in the region $|b| \leq 1.5$, which was observed many times. However, stray radiation from the far sidelobes can cause spurious emission with amplitudes as high as ~ 1 K, so low brightness temperature regions should be viewed with caution. As an example of the data quality we display the entire Parkes dataset at a velocity of $v = 34.4$ km s $^{-1}$ in Figures 3. These images show the variety of size scales represented in the Parkes data alone.

5.2. Combined Parkes and ATCA Cubes

A description and samples of the final combined Parkes and ATCA cubes are presented here. The data are available from the ATNF H I Surveys Archive. The cube sizes, center positions, line-free rms noise per channel and synthesized beam sizes for the continuum subtracted data and data containing continuum emission are given in Tables 3 and 4, respectively. All cubes have 40 arcsec pixels and a channel separation, $\delta v = 0.82 \text{ km s}^{-1}$. The velocity range of the imaged cubes differs from cube to cube. These ranges were chosen to include the bulk of the Galactic emission and minimize cube size for download. The mean rms in the line-free channels is 1.6 K for both the SGPS I and II continuum subtracted cubes. The mean rms for the cubes containing continuum emission is 1.8 K. The positions and dimensions of the combined continuum subtracted cubes are shown in Figure 4.

Because of the large volume of data in the SGPS it is impractical to display all channels of the data cubes here. Instead we have chosen to present only longitude-velocity (l - v) diagrams at $b = 0^\circ$ and an example velocity channel from one of the cubes. The l - v diagrams for SGPS I and II are shown in Figures 5 and 6, respectively. There are approximately 2900 independent spectra in the SGPS I l - v diagram at $b = 0^\circ$ and 300 in the SGPS II l - v diagram at $b = 0^\circ$. Figure 7 is a single velocity channel at $v = 75.05 \text{ km s}^{-1}$ from the continuum subtracted Parkes+ATCA g268 cube, compared with the same velocity channel in the Parkes data alone. This figure shows the dramatic increase in resolution of the SGPS combined image compared with just the single dish data. Figure 7 also demonstrates that the combined data accurately represent the large scale structure present in the single dish data.

5.3. Data Quality and Artifacts

We have taken care to reduce the number of artifacts present in the SGPS data, however there are some artifacts that are unavoidable. These are, in general, artifacts related to gain calibration of the Parkes multibeam and limited u - v coverage in the ATCA data. The Parkes data have some residual longitudinal striping caused by inter-beam gain variations in the multibeam and errors in the estimation of the system temperature, T_{sys} , as explained in §2.2. For the continuum subtracted cubes, errors due to T_{sys} are subtracted, leaving only gain variations. These variations are least evident in the region $|b| \leq 1^\circ 5$, which was observed many times, but are apparent in the higher latitude data. For the cubes containing continuum emission, errors in the estimation of T_{sys} effect the reliability of brightness temperature values on the largest angular scales. Once again, this problem is mitigated for data in the region $|b| \leq 1^\circ 5$ where ten independently calibrated datasets were averaged together.

The Parkes cubes also contain some artifacts related to saturation. There are four positions along the Galactic plane where strong continuum emission saturated the data samplers at Parkes. At these positions the observed fluxes are unreliable so we have blanked the images. These appear as white spots in Figure 3.

The ATCA data suffer from artifacts resulting from a limited number of snapshots and incomplete u - v coverage. Because the interferometric data contain a small number (usually ~ 40) of short duration hour-angle cuts these data have a dynamic range of about 150:1. For Galactic plane H I emission the measured brightness temperature is generally less than 150 K so the images are sensitivity limited, not dynamic range limited. However, towards the numerous bright continuum sources in the Galactic plane, the dynamic range is the fundamental limitation. These continuum sources appear in absorption in the continuum subtracted data where they can limit the images as much as in the non-continuum subtracted data. The limited u - v coverage also leads to a number of radial and azimuthal sidelobe artifacts around bright continuum sources that are not fully removed by the deconvolution process. The SGPS I data suffer from effects related to the fact that all baselines are multiples of 15.3 m. The result is a grating lobe of radius 0.8° around strong continuum sources. The addition of the Parkes data to the interferometric images reduces the effect of the grating lobe but it remains at a level of about 5% of the continuum peak. This artifact is further reduced in the SGPS II cubes, which contain north-south hybrid arrays with a wider variety of baseline spacings.

6. Discussion

SGPS data can be applied to a number of scientific applications that demand high-resolution H I imaging of large areas. In the Galactic ISM many structures are large and have complex interrelationships, which are not apparent from more piecemeal observations. It is in these studies that the SGPS can excel, revealing fine detail that would not have been observed in the large single dish surveys previously available. However, a realistic 3-dimensional picture of the ISM is only possible if the large-scale flux density is measured, which is not measured in interferometric surveys. The large-scale flux is essential for producing a true estimate of the H I mass and dynamics of the Galaxy and understanding the nature of ISM structures. For example, there are some features which are principally perturbations in velocity space caused by turbulence whereas there are others that have massive density variations (e.g. shells with voids). Purely interferometric surveys, while showing details well, can fail to distinguish between these two types of features.

This paper gives a description of the three data products of the SGPS surveys of the

H I line: Parkes continuum subtracted H I cubes with a resolution of $15'$, combined Parkes and ATCA continuum subtracted H I cubes with a resolution of $2'.2$ and combined Parkes and ATCA cubes with a resolution of $\sim 1'.6$ containing continuum emission. Each of these data products was produced for use in different general scientific purposes. The Parkes H I data, though low resolution, cover an extended latitude range. These data are most useful for large-scale panoramic views of the H I, tracing Galactic structure and studies of discrete structures that extend beyond the thin disk of the Galactic plane. The combined Parkes and ATCA continuum subtracted cubes provide high-resolution H I images with maximum surface brightness sensitivity. These data are best-suited for high-resolution examinations of H I emission structures. The combination of the ATCA data with Parkes data ensures that these cubes can be used to explore the ISM on multi-degree scales. Finally, the combined Parkes ATCA data containing continuum emission provide accurately calibrated data at a slightly higher angular resolution. These data were produced specifically for use in H I absorption studies, which require good knowledge of the continuum flux as well as the H I flux in order to accurately measure optical depth.

7. Conclusions

The Southern Galactic Plane Survey (SGPS) is a major new data resource for Galactic H I astronomy, providing an unprecedented view of H I in the inner Galaxy in the southern hemisphere. As part of the International Galactic Plane Survey, the SGPS contributes to nearly continuous coverage of the 1st, 2nd, and 4th quadrants of the plane of the Galaxy. We have presented the H I data products which are now publicly available via the ATNF H I Surveys archive. The H I data products include Parkes H I cubes with 15 arcmin resolution and ~ 100 mK rms sensitivity covering the area $253^\circ \leq l \leq 20^\circ$ and $|b| \leq 10^\circ$, continuum subtracted combined ATCA and Parkes H I cubes with 2 arcmin resolution and ~ 1.6 K rms sensitivity covering the regions $253^\circ \leq l \leq 358^\circ$, $|b| \leq 1.5$ (SGPS I) and $5^\circ \leq l \leq 20^\circ$, $|b| \leq 1.5$ (SGPS II), and combined ATCA and Parkes H I cubes of the same regions including the continuum emission.

The ATCA and the Parkes Radio Telescope are part of the Australia Telescope which is funded by the Commonwealth of Australia for operation as a National Facility managed by CSIRO. This research was supported by NSF grants AST-9732695 and AST-0307603 to the University of Minnesota and AST-0307358 to Harvard University. Additional support was provided through a NASA Graduate Student Researchers Program (GSRP) Fellowship to N. M. M.-G. while at the University of Minnesota. We would like to thank the staff of the Australia Telescope National Facility for their support of this project, especially M.

Calabretta, R. Haynes, D. McConnell, J. Reynolds, R. Sault, R. Wark, and M. Wieringa.

REFERENCES

- Barnes, D. G. et al. 2001, MNRAS, 322, 486
- Brüns, C., Kerp, J., Staveley-Smith, S., Mebold, U., Putman, M. E., Haynes, R. F., Kalberla, P. M. W., Muller, E., & Filipovic, M. D. 2005, A&A, in press (astro-ph/0411453)
- Dickey, J. M., McClure-Griffiths, N. M., Gaensler, B. M., & Green, A. J. 2003, ApJ, 585, 801
- Dickey, J. M., McClure-Griffiths, N. M., Stanimirović, S., Gaensler, B. M., & Green, A. J. 2001, ApJ, 561, 264
- Dwarakanath, K. S., Carilli, C. L., & Goss, W. M. 2002, ApJ, 567, 940
- Gaensler, B. M., Dickey, J. M., McClure-Griffiths, N. M., Green, A. J., Wieringa, M. H., & Haynes, R. F. 2001, ApJ, 549, 959
- Haverkorn, M., Gaensler, B. M., McClure-Griffiths, N. M., Dickey, J. M., & Green, A. J. 2004, ApJ, 609, 776
- Haynes, R., Staveley-Smith, L., Meb, U., Kalberla, P., Jones, K., White, G., Jones, P., Filipovic, M., Dickey, J., & Green, A. 1999, in IAU Symp. 190: New Views of the Magellanic Clouds, Vol. 190, 108
- Heiles, C. & Troland, T. H. 2003, ApJ, 586, 1067
- Kalberla, P. M. W., Mebold, U., & Reich, W. 1980, A&A, 82, 275
- Kalberla, P. M. W., Mebold, U., & Reif, K. 1982, A&A, 106, 190
- Kavars, D., Dickey, J. M., McClure-Griffiths, N. M., Gaensler, B. M., & Green, A. J. 2003, ApJ, 598, 1048
- . 2004, ApJ, submitted
- McClure-Griffiths, N. M. 2001, PhD thesis, University of Minnesota
- McClure-Griffiths, N. M., Dickey, J. M., Gaensler, B. M., & Green, A. J. 2001a, ApJ, 562, 424

- . 2002, *ApJ*, 578, 176
- . 2003, *ApJ*, 594, 833
- . 2004, *ApJ*, 607, L127
- McClure-Griffiths, N. M., Dickey, J. M., Gaensler, B. M., Green, A. J., Haynes, R. F., & Wieringa, M. H. 2000, *AJ*, 119, 2828
- McClure-Griffiths, N. M., Green, A. J., Dickey, J. M., Gaensler, B. M., Haynes, R. F., & Wieringa, M. H. 2001b, *ApJ*, 551, 394
- McKee, C. F. & Ostriker, J. P. 1977, *ApJ*, 218, 148
- Reynolds, J. E. 1994, ATNF Technical Document Series, Tech. Rep. AT/39.3/0400, Australia Telescope National Facility, Sydney
- Sault, R. J. 1994, *A&AS*, 107, 55
- Sault, R. J. & Killeen, N. E. B. 2004, *The MIRIAD User's Guide*, Australia Telescope National Facility, Sydney
- Sault, R. J., Staveley-Smith, L., & Brouw, W. N. 1996, *A&AS*, 120, 375
- Stanimirović, S. 2002, in *ASP Conf. Ser. 278: Single-Dish Radio Astronomy: Techniques and Applications*, 375–396
- Staveley-Smith, L., Wilson, W. E., Bird, T. S., Disney, M. J., Ekers, R. D., Freeman, K. C., Haynes, R. F., Sinclair, M. W., Vaile, R. A., Webster, R. L., & Wright, A. E. 1996, *Publications of the Astronomical Society of Australia*, 13, 243
- Taylor, A. R., Gibson, S. J., Peracaula, M., Martin, P. G., Landecker, T. L., Brunt, C. M., Dewdney, P. E., Dougherty, S. M., Gray, A. D., Higgs, L. A., Kerton, C. R., Knee, L. B. G., Kothes, R., Purton, C. R., Uyaniker, B., Wallace, B. J., Willis, A. G., & Durand, D. 2003, *AJ*, 125, 3145
- Taylor, A. R., Stil, J., Dickey, J., McClure-Griffiths, N., Martin, P., Rotwell, T., & Lockman, J. 2002, in *ASP Conf. Ser. 276: Seeing Through the Dust: The Detection of HI and the Exploration of the ISM in Galaxies*, 68
- Williams, D. R. W. 1973, *A&AS*, 8, 505

Table 1. Basic parameters for the SGPS H I survey

Dataset	Angular Resolution	Spectral Resolution	Longitude coverage	Latitude coverage	1- σ Sensitivity
Parkes SGPS	15'	0.8 km s ⁻¹	253° ≤ l ≤ 20°	b ≤ 10°	180 mK (60 mK ^a)
ATCA + Parkes SGPS I	2'2	0.8 km s ⁻¹	253° ≤ l ≤ 358°	b ≤ 1°5	~ 1.6 K
ATCA + Parkes SGPS II	~ 3'3	0.8 km s ⁻¹	5° ≤ l ≤ 20°	b ≤ 1°5	~ 1.6 K

^aThe rms in the latitude range | b | ≤ 1°5.

Table 2. Cube properties for the Parkes H I Cubes. Column headings are as follows: Cube name; center Galactic longitude, l ; center Galactic latitude, b ; longitude pixel size, δl , latitude pixel size, δb ; number of pixels in l , npix_l ; number of pixels in b , npix_b ; longitude coverage, Δl ; latitude coverage, Δb ; minimum velocity, v_{min} ; maximum velocity, v_{max} ; velocity channel width, δv ; and cube rms.

cube	l ($^{\circ}$)	b ($^{\circ}$)	δl ($'$)	npix_l	δb ($'$)	npix_b	Δl ($^{\circ}$)	Δb ($^{\circ}$)	v_{min} (km s^{-1})	v_{max} (km s^{-1})	δv (km s^{-1})	rms (mK)
p268	264.5	0.0	4	345	4	305	23.00	20.33	-149.8	220.4	0.82	130
p278	277.5	0.0	4	255	4	305	17.00	20.33	-149.8	250.0	0.82	130
p288	287.8	0.0	4	255	4	305	17.00	20.33	-180.3	250.0	0.82	140
p298	297.5	0.0	4	220	4	300	14.67	20.0	-200.1	199.7	0.82	200
p308	307.5	0.0	4	220	4	300	14.67	20.0	-200.1	199.7	0.82	210
p318	317.5	0.0	4	225	4	300	15.00	20.0	-350.2	349.8	0.82	200
p328	327.5	0.0	4	225	4	300	15.00	20.0	-200.1	250.0	0.82	200
p338	337.5	0.0	4	220	4	300	14.67	20.0	-299.9	300.3	0.82	230
p348	347.5	0.0	4	225	4	300	15.00	20.0	-299.9	199.7	0.82	190
p358	357.5	0.0	4	225	4	300	15.00	20.0	-299.9	199.7	0.82	180
p003	3.0	0.0	4	249	4	300	16.60	20.0	-399.6	381.1	0.82	170
p015	15.0	0.0	4	225	4	300	15.00	20.0	-149.8	300.3	0.82	220

Table 3. Properties of the ATCA and Parkes combined H I continuum subtracted cubes. Column headings are as follows: Cube name; center Galactic longitude, l ; center Galactic latitude, b ; longitude pixel size, δl , latitude pixel size, δb ; number of pixels in l , npix_l ; number of pixels in b , npix_b ; longitude coverage, Δl ; latitude coverage, Δb ; minimum velocity, v_{min} ; maximum velocity, v_{max} ; velocity channel width, δv ; synthesized beam size, θ ; and the cube per channel rms.

cube	l ($^{\circ}$)	b ($^{\circ}$)	δl ($''$)	npix_l	δb ($''$)	npix_b	Δl ($^{\circ}$)	Δb ($^{\circ}$)	v_{min} (km s^{-1})	v_{max} (km s^{-1})	δv (km s^{-1})	θ ($'' \times ''$)	rms (K)
g258	257.9	0.0	40	990	40	260	11.00	2.89	-112.1	216.8	0.82	130×130	1.4
g268	267.9	0.0	40	990	40	260	11.00	2.89	-131.9	197.0	0.82	130×130	1.4
g278	277.9	0.0	40	990	40	260	11.00	2.89	-99.8	229.2	0.82	130×130	1.3
g288	287.9	0.0	40	990	40	260	11.00	2.89	-112.1	216.8	0.82	130×130	1.6
g298	297.9	0.0	40	990	40	260	11.00	2.89	-132.7	196.2	0.82	130×130	1.4
g308	307.9	0.0	40	990	40	260	11.00	2.89	-145.1	183.9	0.82	130×130	1.5
g318	317.9	0.0	40	990	40	260	11.00	2.89	-161.6	167.4	0.82	130×130	1.6
g328	327.9	0.0	40	990	40	260	11.00	2.89	-186.3	142.6	0.82	130×130	1.7
g338	337.9	0.0	40	990	40	260	11.00	2.89	-202.8	126.1	0.82	130×130	1.9
g348	347.9	0.0	40	990	40	260	11.00	2.89	-247.3	164.9	0.82	130×130	1.9
g353	353.0	0.0	40	990	40	260	11.00	2.89	-300.1	150.0	0.82	145×90	2.6
g010	10.0	0.0	40	853	40	260	9.48	2.89	-145.1	266.3	0.82	160×110	1.8
g015	16.8	0.0	40	660	40	260	7.33	2.89	-128.6	200.3	0.82	200×130	1.4

Table 4. Properties of the ATCA and Parkes combined H I cubes containing continuum emission. Column headings are the same as in Table 3.

cube	l ($^{\circ}$)	b ($^{\circ}$)	δl ($''$)	npix $_l$	δb ($''$)	npix $_b$	Δl ($^{\circ}$)	Δb ($^{\circ}$)	v_{min} (km s $^{-1}$)	v_{max} (km s $^{-1}$)	δv (km s $^{-1}$)	θ ($'' \times ''$)	rms (K)
g255	255.4	0.0	-0	721	30	351	-6.0	2.9	-227.5	265.5	0.82	143 \times 110	1.2
g260	260.4	0.0	30	721	30	351	-6.0	2.9	-227.5	265.5	0.82	124 \times 120	1.4
g265	265.5	0.0	30	721	30	351	-6.0	2.9	-227.5	265.5	0.82	138 \times 110	1.8
g270	270.4	0.0	30	721	30	361	-6.0	3.0	-227.5	265.5	0.82	132 \times 114	1.1
g275	275.4	0.0	30	721	30	361	-6.0	3.0	-227.5	265.5	0.82	131 \times 116	1.2
g280	280.4	0.0	30	721	30	346	6.0	2.9	-227.5	265.5	0.82	133 \times 112	1.2
g285	285.4	0.0	30	721	30	351	6.0	2.9	-227.5	265.5	0.82	126 \times 115	1.8
g290	290.4	0.0	30	721	30	351	6.0	2.9	-227.5	265.5	0.82	129 \times 112	1.5
g295	295.4	0.0	30	721	30	351	6.0	2.9	-227.5	265.5	0.82	123 \times 116	1.4
g300	300.4	0.0	30	721	30	351	6.0	2.9	-227.5	265.5	0.82	124 \times 113	1.6
g305	305.4	0.0	30	721	30	351	6.0	2.9	-227.5	265.5	0.82	135 \times 112	1.3
g310	310.4	0.0	30	717	30	348	6.0	2.9	-227.5	265.5	0.82	131 \times 119	1.8
g315	315.4	0.0	30	716	30	346	6.0	2.9	-227.5	265.5	0.82	131 \times 116	1.7
g320	320.4	0.0	30	721	30	346	6.0	2.9	-227.5	265.5	0.82	129 \times 119	1.7
g325	325.4	0.0	30	721	30	351	6.0	2.9	-227.5	265.5	0.82	142 \times 117	1.7
g330	330.4	0.0	30	721	30	356	6.0	3.0	-227.5	265.5	0.82	129 \times 115	2.2
g335	335.4	0.0	30	716	30	351	6.0	2.9	-227.5	265.5	0.82	137 \times 126	2.2
g340	340.4	0.0	30	716	30	351	6.0	2.9	-227.5	265.5	0.82	127 \times 121	2.1
g345	345.4	0.0	30	716	30	346	6.0	2.9	-227.5	265.5	0.82	147 \times 114	2.6
g350	350.4	0.0	30	716	30	351	6.0	2.4	-227.5	265.5	0.82	152 \times 108	2.4
g355	355.6	0.0	30	761	30	351	6.3	2.9	-227.5	265.5	0.82	161 \times 108	3.4
g010	9.5	0.0	30	1200	30	350	10.0	2.9	-227.5	265.5	0.82	190 \times 93	2.0
g015	16.5	0.0	30	860	30	350	7.2	2.9	-227.5	265.5	0.82	210 \times 92	1.9

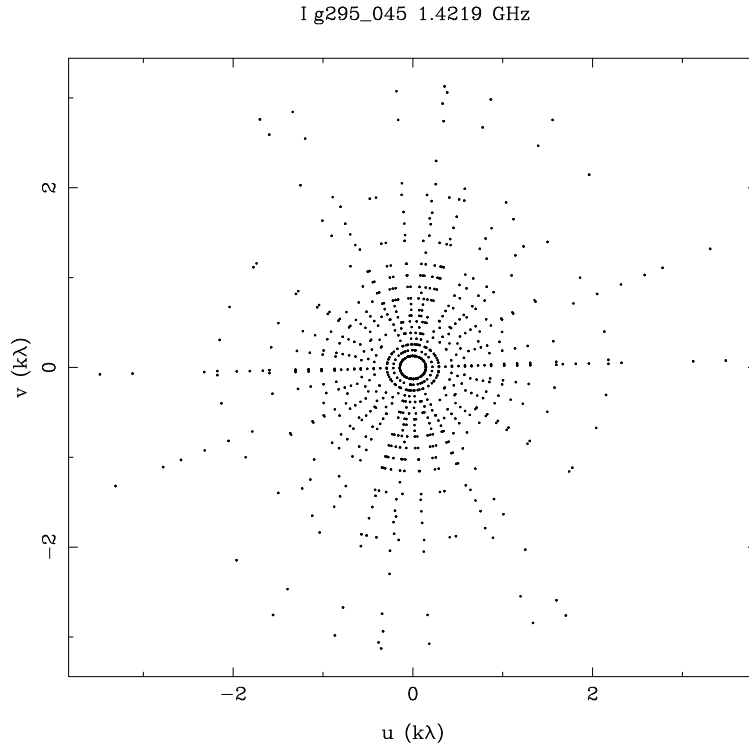


Fig. 1.— The u - v coverage for a typical SGPS I pointing in the field g295. The 6 km antenna has been omitted from this plot to show the coverage of the inner u - v plane. These data use only the east-west configurations of the ATCA.

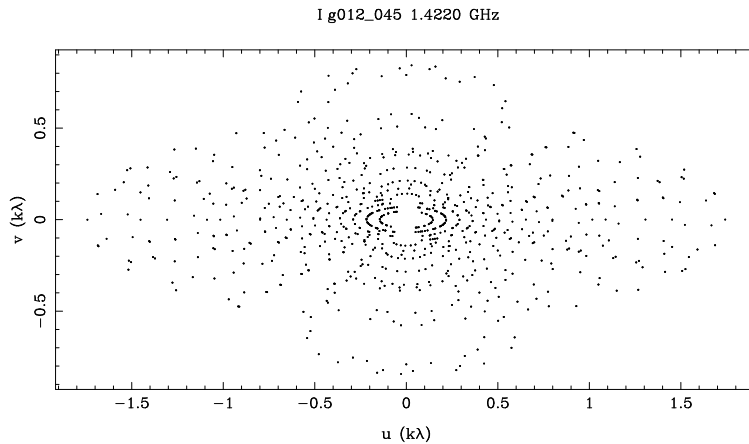


Fig. 2.— The u - v coverage for a typical SGPS II pointing in the field g012. The 6 km antenna has been omitted from this plot to show the coverage of the inner u - v plane. The u - v coverage of this pointing differs from the coverage shown in Figure 1 because of the use of the north-south hybrid arrays in SGPS II and the lower declination of the field.

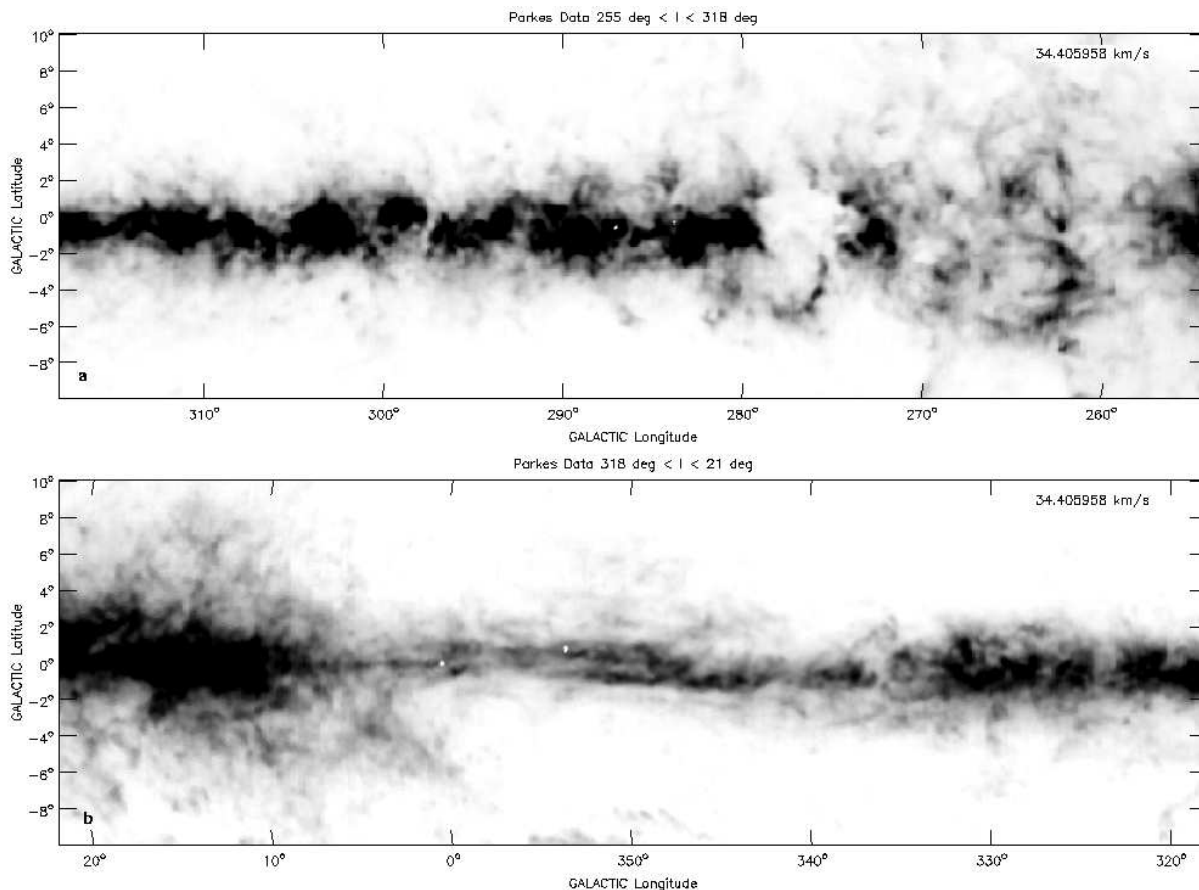


Fig. 3.— Parkes data at $v = 34.4 \text{ km s}^{-1}$ for the region $255^\circ \leq l \leq 318^\circ$ (a) and $318^\circ \leq l \leq 21^\circ$ (b). The greyscale is linear from 3 to 100 K and has been intentionally saturated to bring out the low-level emission.

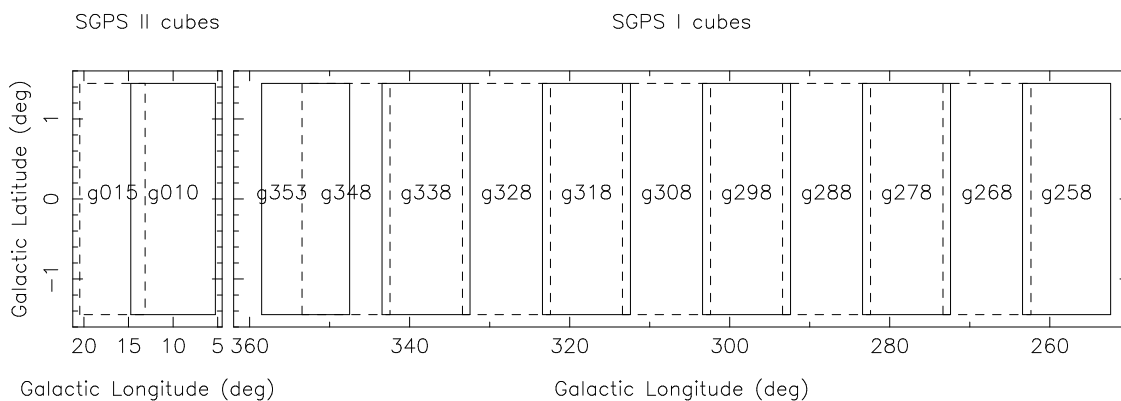


Fig. 4.— Coverage of the SGPS I & II continuum subtracted combined cubes. Field names are the names used for the data cubes as released and as given in Table 3.

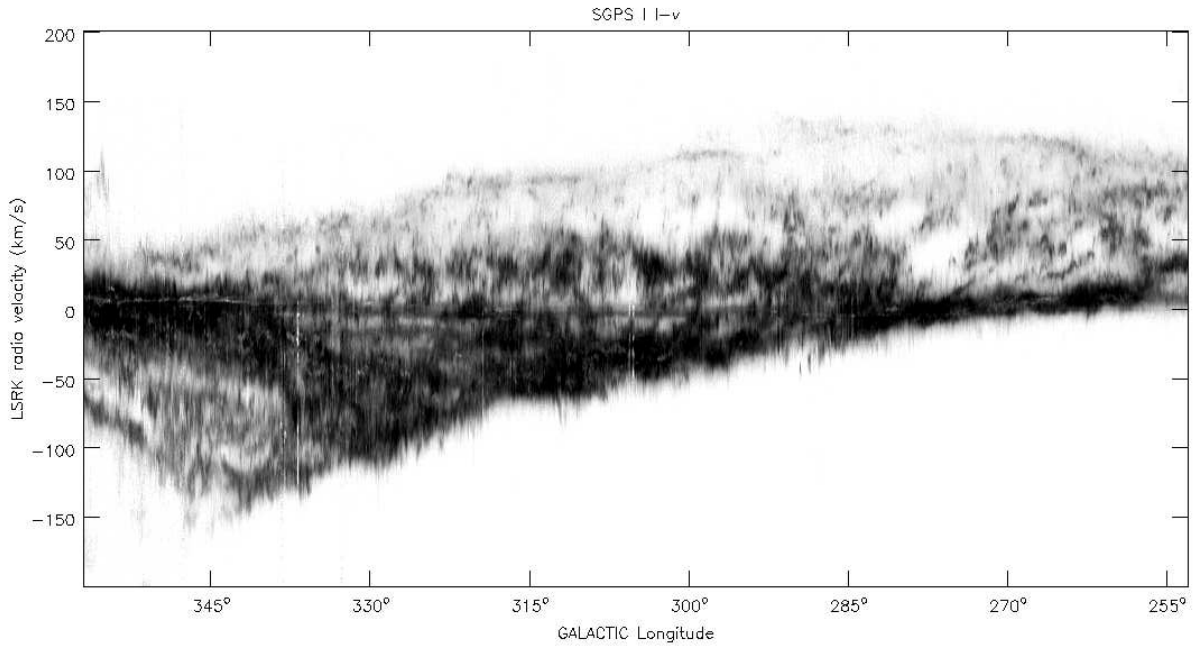


Fig. 5.— Longitude-velocity diagram of continuum subtracted data for the SGPS I region at $b = 0^\circ$. The greyscale runs from 3 to 120 K and uses a square-root transfer function. The occasional white vertical stripes (e.g. near $l = 306^\circ$) in the image are the result of H I absorption towards strong continuum sources that have been subtracted. Similarly, the horizontal stripes, especially near $v = 0 \text{ km s}^{-1}$ are due to H I self-absorption in the local gas.

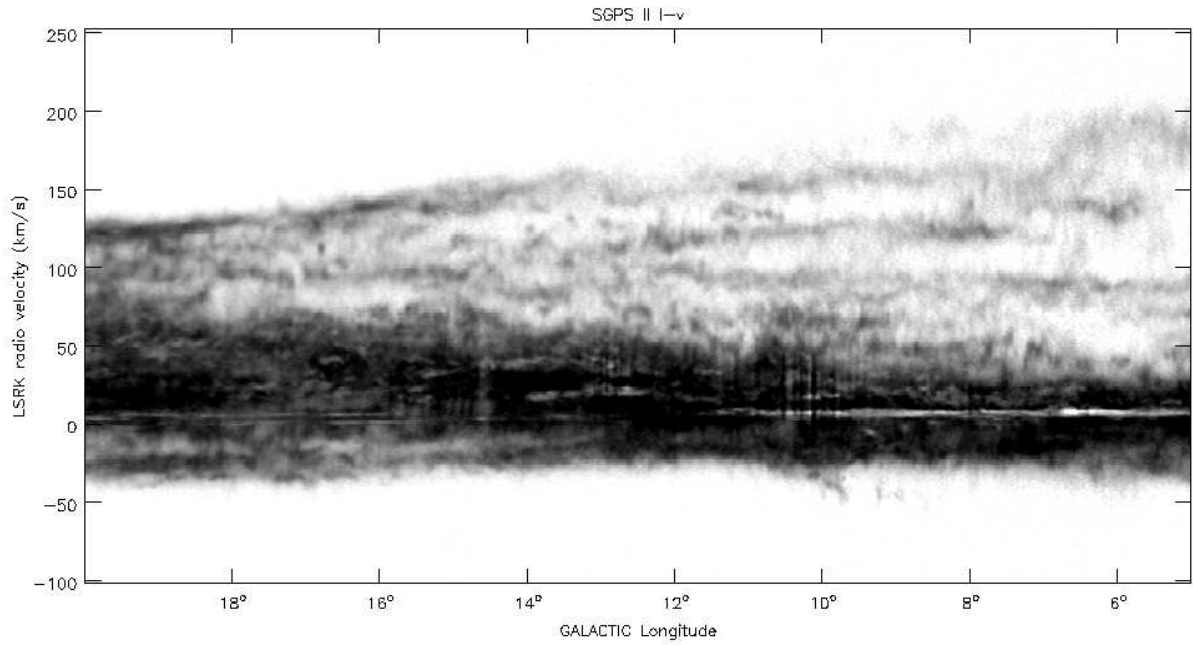


Fig. 6.— Longitude-velocity diagram of continuum subtracted data for the SGPS II region at $b = 0^\circ$. The greyscale runs from 3 to 120 K and uses a square-root transfer function. As in Figure 5, the vertical stripes seen here are due to continuum absorption and the horizontal stripes near $v = 0 \text{ km s}^{-1}$ are due to H I self-absorption.

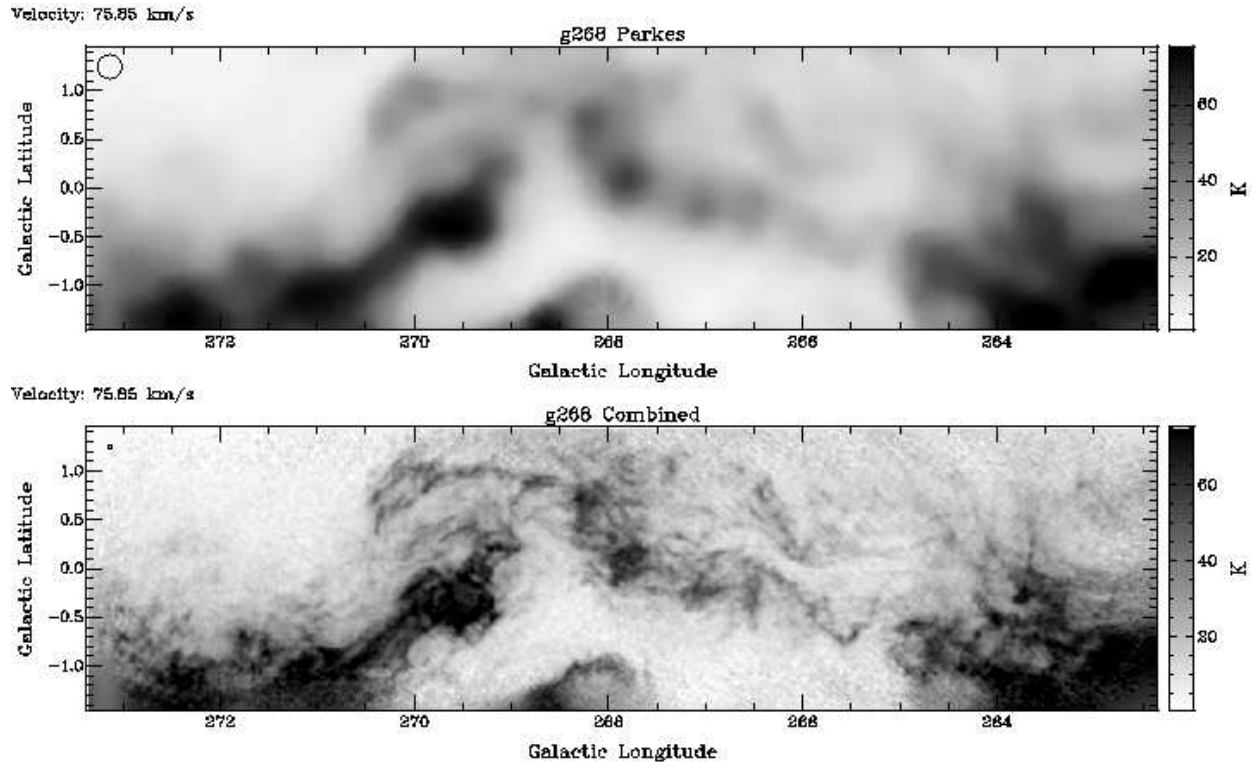


Fig. 7.— Comparison of Parkes and Combined data for the g268 cube at $v = 75.05 \text{ km s}^{-1}$. The beam size is marked as an open circle in the upper left-hand corner of each image. The greyscale is the same for the two panels, running linearly from 1 to 75 K.